International Journal of Fracture **70:** 147–165, 1995.

Singular integral equation method in optimization of stress-relieving hole: a new approach based on the body force method

NAO-AKI NODA and TADATOSHI MATSUO
Mechanical Engineering Department, Kyushu Institute of Technology, Kitakyushu 804, Japan

Received: 8 September 1993; accepted in revised form 30 September 1994

Abstract. This paper is concerned with a method of decreasing stress concentration due to a notch and a hole by providing additional holes in the region of the principal notch or hole. A singular integral equation method that is useful for this optimization problem is discussed. To formulate the problem the idea of the body force method is applied using the Green's function for a point force as a fundamental solution. Then, the interaction problem between the principal notch and the additional holes is expressed as a system of singular integral equations with a Cauchy-type singular kernel, where densities of the body force distribution in the x- and y-directions are to be unknown functions. In solving the integral equations, eight kinds of fundamental density functions are applied; then, the continuously varying unknown functions of body force densities are approximated by a linear combination of products of the fundamental density functions and polynomials. In the searching process of the optimum conditions, the direction search of Hooke and Jeeves is employed. The calculation shows that the present method gives the stress distribution along the boundary of a hole very accurately with a short CPU time. The optimum position and the optimum size of the auxiliary hole are also determined efficiently with high accuracy.

1. Introduction

It is desirable in many designs to reduce weight and minimize stress concentration due to notches and holes. One way to achieve this is by providing additional holes as stress-relieving holes in the region of the principal notch and hole [1, 2]. Recently, several investigators have applied various numerical methods to optimize the geometrical shape of machine components [3–7]. In general, optimization can be achieved through gradual change of the respective geometrical shapes and comparison of the maximum local stresses. Usually, the magnitude and the position of the maximum stress varies slightly with a change in the respective geometrical conditions; thus, it is necessary to calculate very accurate stress distributions along the boundary of the components. However, it is very difficult to accurately obtain the smooth stress distribution by applying most numerical methods and eventually few reliable results are available in the optimum geometry.

In previous papers, the numerical solutions of the singular integral equation of the body force method in crack problems have been discussed [8–11]. In those papers unknown functions of the body force densities have been approximated by the products of fundamental density functions and polynomials. It was found that this new method gives results with better accuracy in shorter CPU time compared to the conventional body force method using step-functions [8–11].

In this paper a singular integral equation method in the analysis of interaction problems between notches and holes is discussed. To formulate the problem the body force method is applied, where the Green's functions for point forces are used as the fundamental solution. It

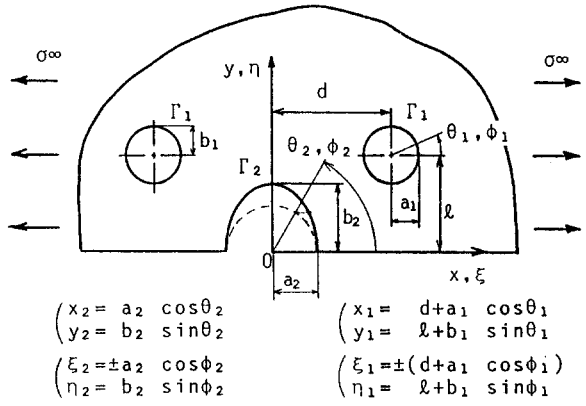

Fig. 1. Two stress-relieving holes and semi-elliptical notch in a semi-infinite plate.

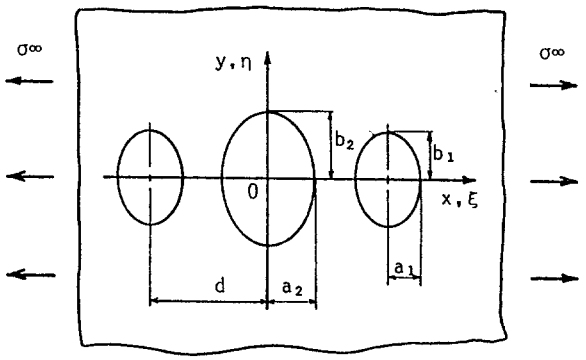

Fig. 2. Two stress-relieving holes and elliptical hole in an infinite plate.

will be shown that the present method is very useful for analyzing optimization problems for an additional hole, and that the solution will be given with higher accuracy compared with that of other methods. In this paper optimum conditions will be considered for several problems shown in Figs. 1–3.

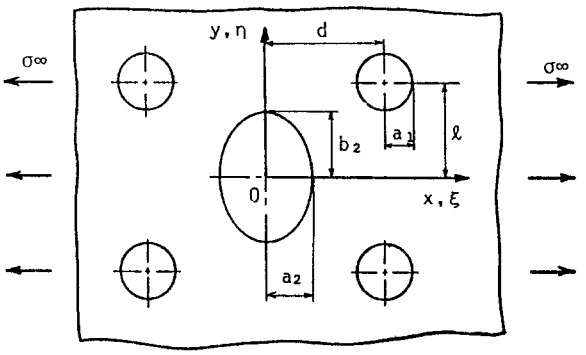

Fig. 3. Four stress-relieving holes and elliptical hole in an infinite plate.

2. Singular integral equations of the body force method

In the solutions of the conventional body force method [12–14] stress concentration problems are reduced to determining the densities of the body force, that is, the continuously embedded point forces along the prospective boundary. In the conventional method the unknown function of the body force densities is approximated by the product of the fundamental density functions and the step-functions. The method has been widely applied to various notch and crack problems. However, an accurate stress distribution is difficult to calculate along the boundaries because of the step-functions used.

In this paper first the singular integral equation technique of using the body force method in the interaction between a notch and additional holes is shown and considered. Here, a semi-infinite plate with a semi-elliptical notch ($x = a_2 \cos\theta_2$, $y = b_2 \sin\theta_2$) and additional stress-relieving elliptical holes [$x = \pm(d + a_1 \cos\theta_1)$, $y = l + b_1 \sin\theta_1$ ($a_1 = b_1$)] is taken as an example to explain the numerical solution (see Fig. 1). The problem can be formulated in terms of singular integral equations by using a Green's function, that is, the stress field at an arbitrary point (x, y) when point forces act symmetrically on the two points $(\pm\xi, \eta)$ in the semi-infinite plate. The formulation is based on the principle of superposition. The integral equation is expressed by (1), where the body force densities distributed along the prospective boundaries in the x-, y-directions $\rho_x^*(\phi_k)$, $\rho_y^*(\phi_k)$ ($k = 1, 2$) are to be unknown functions ($k = 1$: for additional hole, $k = 2$: for principal notch). Here, ϕ_k is the angle that specifies the points where the body forces are distributed.

$$-\tfrac{1}{2}\{\rho_x^*(\theta_i)\cos\theta_{i0} + \rho_y^*(\theta_i)\sin\theta_{i0}\} + \sum_{k=1}^{2}\int_{\Gamma_k} K_{nn}^{Fx}(\phi_k, \theta_i)\rho_x^*(\phi_k)\,ds + \sum_{k=1}^{2}\int_{\Gamma_k} K_{nn}^{Fy}(\phi_k, \theta_i)\rho_y^*(\phi_k)\,ds = -\sigma^{\infty}\cos^2\theta_{i0}, \tag{1a}$$

$$-\tfrac{1}{2}\{-\rho_x^*(\theta_i)\sin\theta_{i0} + \rho_y^*(\theta_i)\cos\theta_{i0}\} + \sum_{k=1}^{2}\int_{\Gamma_k} K_{nt}^{Fx}(\phi_k, \theta_i)\rho_x^*(\phi_k)\,ds + \sum_{k=1}^{2}\int_{\Gamma_k} K_{nt}^{Fy}(\phi_k, \theta_i)\rho_y^*(\phi_k)\,ds = \sigma^{\infty}\sin\theta_{i0}\cos\theta_{i0}, \tag{1b}$$

(for additional notch $i = 1: 0 \leqslant \theta_1 \leqslant 2\pi$),

(for principal notch $i = 2: 0 \leqslant \theta_2 \leqslant \tfrac{1}{2}\pi$),

where

$$-d\xi = a_k \sin\phi_k d\phi_k,\ d\eta = b_k \cos\phi_k d\phi_k,$$
$$ds = \sqrt{a_k^2 \sin^2\phi_k + b_k \cos^2\phi_k}\,d\phi_k \tan\theta_{i0} = (a_k/b_k)\tan\theta_i. \tag{2}$$

θ_{i0} is the angle between the x-axis and the normal direction at the point (x, y) on the ellipse. $\sum_{k=1}^{2}$ means the summation of integrating the body force density on the prospective boundary of the additional elliptical holes and the semi-elliptical notch.

Equations (1) are virtually the boundary conditions at the imaginary boundary $\Gamma_i (i = 1, 2)$; that is, $\sigma_n = 0$ and $\tau_{nt} = 0$. The first terms of (1) represent the stress due to the body force distributed on the $\ominus$ boundary. The $\ominus$ boundary means the imaginary boundary composed of the internal points that are infinitesimally apart from the initial boundary [12]. Taking $K_{nn}^{Fx}(\phi_k, \theta_i)$ for example, the notation means the normal stress σ_n induced at the point when the body force with unit density in the x-direction is acting at the infinitesimal arc length on the kth elliptical boundary. These kernels include the singular terms having the singularity of the form $1/\sin\{(\theta_i - \phi_i)/2\}$ in the case $i = k$ [17]. In this case $\theta_i = \phi_i$, the integration should be interpreted as the meaning of Cauchy's principle values.

3. Numerical solution of the conventional body force method

First, the conventional body force method will be explained through the numerical solution of the singular integral equation (1). The unknown functions in (1) $\rho_x^*(\phi_k)$, $\rho_y^*(\phi_k)$ are defined by the following equations,

$$\begin{aligned} \rho_x^*(\phi_k) &= \frac{\mathrm{d}F_\xi}{\mathrm{d}s} = \frac{\mathrm{d}F_\xi}{\mathrm{d}\eta} n_x(\phi_k) = \rho_x(\phi_k) n_x(\phi_k), \\ \rho_y^*(\phi_k) &= \frac{\mathrm{d}F_\eta}{\mathrm{d}s} = -\frac{\mathrm{d}F_\eta}{\mathrm{d}\xi} n_y(\phi_k) = \rho_y(\phi_k) n_y(\phi_k), \end{aligned} \tag{3}$$

where $\mathrm{d}F_\xi$, $\mathrm{d}F_\eta$ are the components of the resultant of the body force in the x-, y-directions acting on the infinitesimal arc length $\mathrm{d}s$, respectively. Here, $n_x(\phi_k)$, $n_y(\phi_k)$ are the x, y components [$= (\cos\theta_{k0}, \sin\theta_{k0})$] of the normal unit vector respectively at the point (x_k, y_k). They are expressed by the following equations

$$n_x(\phi_k) = \frac{b_k \cos\phi_k}{\sqrt{a_k^2 \sin^2\phi_k + b_k^2 \cos^2\phi_k}}, \quad n_y(\phi_k) = \frac{a_k \sin\phi_k}{\sqrt{a_k^2 \sin^2\phi_k + b_k^2 \cos^2\theta_k}}, \tag{4}$$

where $\rho_x(\phi_k)$, $\rho_y(\phi_k)$ are the body force density of the unit projected length in the x-, y-directions [15, 16],

$$\rho_x(\phi_k) = \frac{\mathrm{d}F_\xi}{\mathrm{d}\eta}, \quad \rho_y(\phi_k) = -\frac{\mathrm{d}F_\eta}{\mathrm{d}\xi}. \tag{5}$$

Using the expression of (3), the singular integral equations (1) become the following equations

$$\begin{aligned} &-\tfrac{1}{2}\{\rho_x(\theta_i)\cos^2\theta_{i0} + \rho_y(\phi_i)\sin^2\theta_{i0}\} + \sum_{k=1}^{2}\int_{\Gamma_k} K_{nn}^{Fx}(\phi_k, \theta_i)\rho_x(\phi_k) b_k \cos\phi_k \,\mathrm{d}\phi_k \\ &+\sum_{k=1}^{2}\int_{\Gamma_k} K_{nn}^{Fy}(\phi_k, \theta_i)\rho_y(\phi_k)\, a_k \sin\phi_k \,\mathrm{d}\phi_k = -\sigma^\infty \cos^2\theta_{i0}, \end{aligned} \tag{6a}$$

$$\begin{aligned} &-\tfrac{1}{2}\{-\rho_x(\theta_i) + \rho_y(\theta_i)\}\sin\theta_{i0}\cos\theta_{i0} + \sum_{k=1}^{2}\int_{\Gamma_k} K_{nt}^{Fx}(\phi_k, \theta_i)\rho_x(\phi_k) b_k \cos\phi_k \,\mathrm{d}\phi_k \\ &+\sum_{k=1}^{2}\int_{\Gamma_k} K_{nt}^{Fy}(\phi_k, \theta_i)\rho_y(\phi_k)\, a_k \sin\phi_k \,\mathrm{d}\phi_k = \sigma^\infty \sin\theta_{i0}\cos\theta_{i0}, \end{aligned}$$

$$\begin{aligned}&(\text{for additional notch } i = 1: 0 \leqslant \theta_1 \leqslant 2\pi),\\ &(\text{for principal notch } i = 2: 0 \leqslant \theta_2 \leqslant \tfrac{1}{2}\pi).\end{aligned} \tag{6b}$$

It should be noted that $n_x(\phi_k)$, $n_y(\phi_k)$ are regarded as a kind of fundamental density function to approximate $\rho_x^*(\phi_k)$, $\rho_y^*(\phi_k)$ very accurately. They are the exact densities of the body forces for the problem of an isolated elliptical hole in an infinite plate under tension [12, 13]. In the conventional body force method, then, the unknown weighting functions $\rho_x(\phi_k)$, $\rho_y(\phi_k)$ have been approximated by the stepped functions, while in this paper, the numerical solution described in the following sections will be used.

4. Definition of new fundamental density functions

The fundamental density functions for the body forces in the x-directional $w_x(\phi_k)$ and the ones in the y-direction $w_y(\phi_k)$ are defined by the following expression [15–17]

$$\begin{aligned}w_{x1}(\phi_\kappa) &= n_x(\phi_\kappa)/\cos\,\phi_\kappa,\\ w_{x2}(\phi_\kappa) &= n_x(\phi_\kappa)\,\tan\,\phi_\kappa,\\ w_{x3}(\phi_\kappa) &= n_x(\phi_\kappa),\\ w_{x4}(\phi_\kappa) &= n_x(\phi_\kappa)\,\sin\,\phi_\kappa,\end{aligned} \tag{7a}$$

$$\begin{aligned}w_{y1}(\phi_\kappa) &= n_y(\phi_\kappa)/\sin\,\phi_\kappa,\\ w_{y2}(\phi_\kappa) &= n_y(\phi_\kappa),\\ w_{y3}(\phi_\kappa) &= n_y(\phi_\kappa)\,\cot\,\phi_\kappa,\\ w_{y4}(\phi_\kappa) &= n_y(\phi_\kappa)\,\cos\,\phi_\kappa.\end{aligned} \tag{7b}$$

The fundamental density functions defined by (7) are shown in Fig. 4 for the circular boundary.

The unknown functions of the body force densities for additional holes $\rho_x^*(\phi_1)$, $\rho_y^*(\phi_1)$ can be expressed by a linear combination of the fundamental density functions defined by (7) and the weight functions $\rho_{x1}(\phi_k)$, $\rho_{x2}(\phi_k), \ldots, \rho_{y4}(\phi_k)$ as shown in the following equations

$$\begin{aligned}\rho_x^*(\phi_1) &= \rho_{x1}(\phi_1)w_{x1}(\phi_1) + \rho_{x2}(\phi_1)w_{x2}(\phi_1) + \rho_{x3}(\phi_1)w_{x3}(\phi_1)\\ &\quad +\rho_{x4}(\phi_1)w_{x4}(\phi_1),\\ \rho_y^*(\phi_1) &= \rho_{y1}(\phi_1)w_{y1}(\phi_1) + \rho_{y2}(\phi_1)w_{y2}(\phi_1) + \rho_{y3}(\phi_1)w_{y3}(\phi_1)\\ &\quad +\rho_{y4}(\phi_1)w_{y4}(\phi_1).\end{aligned} \tag{8}$$

Using (8), $\rho_x^*(\phi_k)$, $\rho_y^*(\phi_k)$ which are defined in $0 \leqslant \phi_k \leqslant 2\pi$ can be expressed by the weight functions $\rho_{x1}(\phi_k)$, $\rho_{x2}(\phi_k), \ldots, \rho_{y4}(\phi_k)$. These weight functions are symmetric with respect to the axes $\phi_k = 0, \frac{1}{2}\pi, \pi, \frac{3}{2}\pi$.

On the other hand, from the symmetry of the problem the unknown functions of the body force densities for principle notch $\rho_x^*(\phi_2)$, $\rho_y^*(\phi_2)$ which are defined in $0 \leqslant \phi_k \leqslant \frac{1}{2}\pi$ can be simply expressed by the following equations

$$\begin{aligned}\rho_x^*(\phi_2) &= \rho_{x3}(\phi_2)w_{x3}(\phi_2),\\ \rho_y^*(\phi_2) &= \rho_{y2}(\phi_2)w_{y2}(\phi_2).\end{aligned} \tag{9}$$

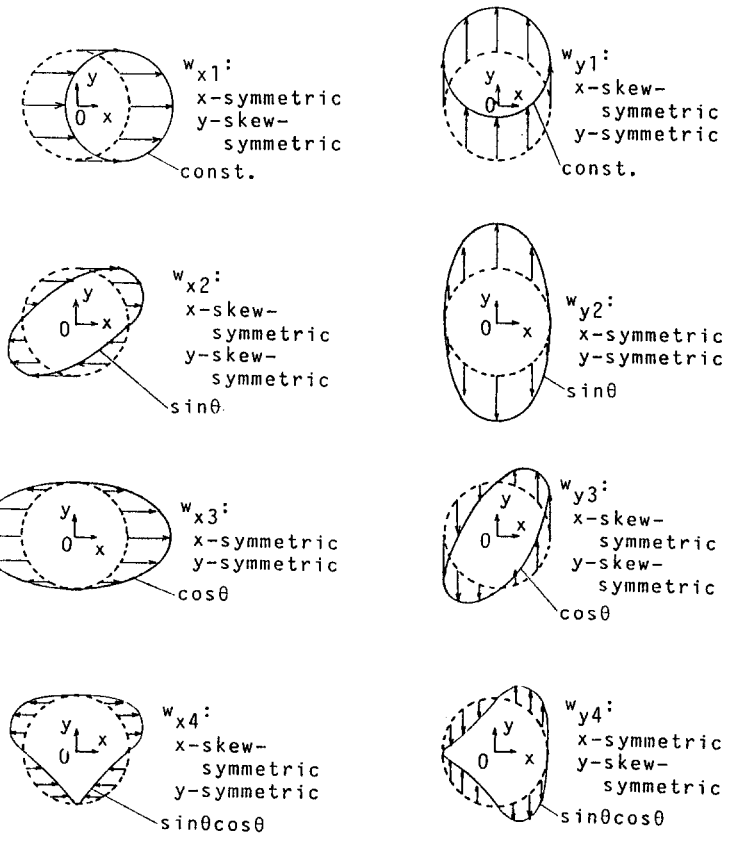

Fig. 4. Fundamental density functions for circular boundaries.

5. Numerical solution of the singular integral equations

Using the expressions in (8) and (9), the singular integral equation (1) is reduced to the following equations (10) instead of (6).

$$
\begin{aligned}
&-\tfrac{1}{2}[\{\rho_{x1}(\theta_1)/\cos\,\theta_1+\rho_{x2}(\theta_1)\,\tan\,\theta_1+\rho_{x3}(\theta_1)+\rho_{x4}(\theta_1)\,\sin\,\theta_1\}\,\cos^2\,\theta_{10}\\
&\quad+\{\rho_{y1}(\theta_1)/\sin\,\theta_1+\rho_{y2}(\theta_1)+\rho_{y3}\,\cot\,(\theta_1)+\rho_{y4}(\theta_1)\,\cos\,\theta_1\}\,\sin^2\,\theta_{10}]\\
&\quad+\int_0^{2\pi}K_{nn}^{Fx}(\phi_1,\,\theta_1)\{\rho_{x1}(\phi_1)/\cos\,\phi_1+\rho_{x2}(\phi_1)\,\tan(\phi_1)+\rho_{x3}(\phi_1)\\
&\quad+\rho_{x4}(\phi_1)\,\sin\,\phi_1\}b_1\,\cos\,\phi_1\,\mathrm{d}\phi_1+\int_0^{2\pi}K_{nn}^{Fy}(\phi_1,\,\theta_1)\{\rho_{y1}(\phi_1)/\sin\,\phi_1+\rho_{y2}(\phi_1)\\
&\quad+\rho_{y3}(\phi_1)\,\cot(\phi_1)+\rho_{y4}(\phi_1)\,\cos\,\phi_1\}a_1\,\sin\,\phi_1\,\mathrm{d}\phi_1\\
&\quad+\int_0^{\frac{1}{2}\pi}K_{nn}^{Fx}(\phi_2,\,\theta_1)\rho_{x3}(\phi_2)b_2\,\cos\,\phi_2\,\mathrm{d}\phi_2\\
&\quad+\int_0^{\frac{1}{2}\pi}K_{nn}^{Fy}(\phi_2,\,\theta_1)\rho_{y2}(\phi_2)a_2\,\sin\,\phi_2\,\mathrm{d}\phi_2\\
&=-\sigma^{\infty}\,\cos^2\,\theta_{10}\quad(\text{for additional hole } i=1{:}\,0\leqslant\theta_1\leqslant 2\pi),
\end{aligned}
$$

$$
\begin{aligned}
&-\tfrac{1}{2}[\{\rho_{x1}(\theta_1)/\cos\theta_1 + \rho_{x2}(\theta_1)\tan\theta_1 + \rho_{x3}(\theta_1) + \rho_{x4}(\theta_1)\sin\theta_1\} \\
&\quad + \{\rho_{y1}(\theta_1)/\sin\theta_1 + \rho_{y2}(\theta_1) + \rho_{y3}\cot(\theta_1) + \rho_{y4}(\theta_1)\cos\theta_1\}]\sin\theta_{10}\cos\theta_{10} \\
&\quad + \int_0^{2\pi} K_{nt}^{Fx}(\phi_1,\theta_1)\{\rho_{x1}(\phi_1)/\cos\phi_1 + \rho_{x2}(\phi_1)\tan(\phi_1) + \rho_{x3}(\phi_1) \\
&\quad + \rho_{x4}(\phi_1)\sin\phi_1\}b_1\cos\phi_1\,\mathrm{d}\phi_1 + \int_0^{2\pi} K_{nt}^{Fy}(\phi_1,\theta_1)\{\rho_{y1}(\phi_1)/\sin\phi_1 \\
&\quad + \rho_{y2}(\phi_1) + \rho_{y3}(\phi_1)\cot(\phi_1) + \rho_{y4}(\phi_1)\cos\phi_1\}a_1\sin\phi_1\,\mathrm{d}\phi_1 \\
&\quad + \int_0^{1/2\pi} K_{nt}^{Fx}(\phi_2,\theta_1)\rho_{x3}(\phi_2)b_2\cos\phi_2\,\mathrm{d}\phi_2 \\
&\quad + \int_0^{1/2\pi} K_{nt}^{Fy}(\phi_2,\theta_1)\rho_{y2}(\phi_2)a_2\sin\phi_2\,\mathrm{d}\phi_2 \\
&\quad = \sigma^{\infty}\cos\theta_{10}\sin\theta_{10} \quad \text{(for additional hole } i = 1\text{: } 0 \leqslant \theta_1 \leqslant 2\pi\text{)}, \\
&-\tfrac{1}{2}[\rho_{x3}(\theta_2)\cos^2\theta_{20} + \rho_{y2}(\theta_2)\sin^2\theta_{20}] \\
&\quad + \int_0^{2\pi} K_{nn}^{Fx}(\phi_1,\theta_2)\{\rho_{x1}(\phi_1)/\cos\phi_1 + \rho_{x2}(\phi_1)\tan(\phi_1) + \rho_{x3}(\phi_1) \\
&\quad + \rho_{x4}(\phi_1)\sin\phi_1\}b_1\cos\phi_1\,\mathrm{d}\phi_1 + \int_0^{2\pi} K_{nn}^{Fy}(\phi_1,\theta_2)\{\rho_{y1}(\phi_1)/\sin\phi_1 \\
&\quad + \rho_{y2}(\phi_1) + \rho_{y3}(\phi_1)\cot(\phi_1) + \rho_{y4}(\phi_1)\cos\phi_1\}a_1\sin\phi_1\,\mathrm{d}\phi_1 \\
&\quad + \int_0^{1/2\pi} K_{nn}^{Fx}(\phi_2,\theta_2)\rho_{x3}(\phi_2)b_2\cos\phi_2\,\mathrm{d}\phi_2 \\
&\quad + \int_0^{1/2\pi} K_{nn}^{Fy}(\phi_2,\theta_2)\rho_{y2}(\phi_2)a_2\sin\phi_2\,\mathrm{d}\phi_2 \\
&\quad = -\sigma^{\infty}\cos^2\theta_{20} \quad \text{(for principal notch } i = 2\text{: } 0 \leqslant \theta_2 \leqslant \tfrac{1}{2}\pi\text{)}, \\
&-\tfrac{1}{2}[-\rho_{x3}(\theta_2) + \rho_{y2}(\theta_2)]\sin\theta_{20}\cos\theta_{20} \\
&\quad + \int_0^{2\pi} K_{nt}^{Fx}(\phi_1,\theta_2)\{\rho_{x1}(\phi_1)/\cos\phi_1 + \rho_{x2}(\phi_1)\tan(\phi_1) + \rho_{x3}(\phi_1) \\
&\quad + \rho_{x4}(\phi_1)\sin\phi_1\}b_1\cos\phi_1\,\mathrm{d}\phi_1 + \int_0^{2\pi} K_{nt}^{Fy}(\phi_1,\theta_2)\{\rho_{y1}(\phi_1)/\sin\phi_1 \\
&\quad + \rho_{y2}(\phi_1) + \rho_{y3}(\phi_1)\cot(\phi_1) + \rho_{y4}(\phi_1)\cos\phi_1\}a_1\sin\phi_1\,\mathrm{d}\phi_1 \\
&\quad + \int_0^{1/2\pi} K_{nt}^{Fx}(\phi_2,\theta_2)\rho_{x3}(\phi_2)b_2\cos\phi_2\,\mathrm{d}\phi_2 \\
&\quad + \int_0^{1/2\pi} K_{nt}^{Fy}(\phi_2,\theta_2)\rho_{y2}(\phi_2)a_2\sin\phi_2\,\mathrm{d}\phi_2 \\
&\quad = \sigma^{\infty}\cos\theta_{20}\sin\theta_{20} \quad \text{(for principal notch } i = 2\text{: } 0 \leqslant \theta_2 \leqslant \tfrac{1}{2}\pi\text{)}. \qquad (10)
\end{aligned}
$$

In the present analysis, polynomials have been used to approximate the unknown functions as continuous function. Now, from the symmetry of the problem the following expression can be applied.

$$\begin{aligned}
\rho_{x1}(\phi_1) &= \sum_{n=1}^{M1/4} a_{1n}t_n(\phi_1), \quad \rho_{x2}(\phi_1) = \sum_{n=1}^{M1/4} b_{1n}t_n(\phi_1), \\
\rho_{x3}(\phi_1) &= \sum_{n=1}^{M1/4} c_{1n}t_n(\phi_1), \quad \rho_{x4}(\phi_1) = \sum_{n=1}^{M1/4} d_{1n}t_n(\phi_1), \\
\rho_{y1}(\phi_1) &= \sum_{n=1}^{M1/4} e_{1n}t_n(\phi_1), \quad \rho_{y2}(\phi_1) = \sum_{n=1}^{M1/4} f_{1n}t_n(\phi_1), \\
\rho_{y3}(\phi_1) &= \sum_{n=1}^{M1/4} g_{1n}t_n(\phi_1), \quad \rho_{y4}(\phi_1) = \sum_{n=1}^{M1/4} h_{1n}t_n(\phi_1),
\end{aligned} \tag{11}$$

$$\rho_{x3}(\phi_2) = \sum_{n=1}^{M2} c_{2n}u_n(\phi_2), \quad \rho_{y2}(\phi_2) = \sum_{n=1}^{M2} f_{2n}u_n(\phi_2), \tag{12}$$

$$t_n(\phi_1) = \cos\{2(n-1)\phi_1\}, \tag{13}$$

$$u_n(\phi_2) = (\tfrac{1}{2}\pi - \phi_2)^{2(n-1)}, \tag{14}$$

where $M1$ is the number of the collocation points for each additional hole in the range $0 \leqslant \phi_1 \leqslant 2\pi$, and $M2$ is the number of the collocation points for the principal hole in the range $0 \leqslant \phi_2 \leqslant \frac{1}{2}\pi$.

Using the approximation method mentioned above, we obtain the following system of linear equations for the determination of the coefficients $a_{1n}, b_{1n}, \ldots, f_{2n}$. The number of unknown coefficients is $2(M1 + M2)$. The convenient sets of the collocation points ($M = 1 \sim M1 + M2$) are given by (15).

$$\begin{aligned}
\theta_1 &= \frac{2\pi}{M1}(M - 0.5) \quad M = 1 \sim M1, \\
\theta_2 &= \frac{\pi}{2 \cdot M2}(M - M1 - 0.5) \quad M = M1 + 1 \sim M1 + M2.
\end{aligned} \tag{15}$$

$$
\begin{aligned}
&\sum_{n=1}^{M1/4}(a_{1n}A_{1n}+b_{1n}B_{1n}+c_{1n}C_{1n}+d_{1n}D_{1n}\\
&\quad +e_{1n}E_{1n}+f_{1n}F_{1n}+g_{1n}G_{1n}+h_{1n}H_{1n})\\
&\quad +\sum_{n=1}^{M2}(c_{2n}C_{2n}+f_{2n}F_{2n})=-\sigma_x^{\infty}\cos^2\theta_0.\\
&\sum_{n=1}^{M1/4}(a_{1n}I_{1n}+b_{1n}J_{1n}+c_{1n}K_{1n}+d_{1n}L_{1n}\\
&\quad +e_{1n}M_{1n}+f_{1n}N_{1n}+g_{1n}O_{1n}+h_{1n}P_{1n})\\
&\quad +\sum_{n=1}^{M2}(c_{2n}K_{2n}+f_{2n}N_{2n})=\sigma_x^{\infty}\cos\theta_0\sin\theta_0.
\end{aligned}
\tag{16}
$$

$$
\begin{aligned}
A_{1n} &= -\tfrac{1}{2}t_n(\theta_1)\cos^2\theta_{10}/\cos\theta_1+\int_0^{2\pi}K_{nn}^{Fx}(\phi_1,\theta_1)t_n(\theta_1)b_1\,\mathrm{d}\theta_1,\\
B_{1n} &= -\tfrac{1}{2}t_n(\theta_1)\cos^2\theta_{10}\tan\theta_1+\int_0^{2\pi}K_{nn}^{Fx}(\phi_1,\theta_1)t_n(\phi_1)b_1\sin\phi_1\,\mathrm{d}\phi_1,\\
C_{1n} &= -\tfrac{1}{2}t_n(\theta_1)\cos^2\theta_{10}+\int_0^{2\pi}K_{nn}^{Fx}(\phi_1,\theta_1)t_n(\phi_1)b_1\cos\phi_1\,\mathrm{d}\phi_1,\\
&\cdots\cdots\\
H_{1n} &= -\tfrac{1}{2}t_n(\theta_1)\sin^2\theta_{10}\cos\theta_1+\int_0^{2\pi}K_{nn}^{Fy}(\phi_1,\theta_1)t_n(\phi_1)b_1\sin(\phi_1)\cos(\phi_1)\,\mathrm{d}\phi_1,\\
C_{2n} &= \int_0^{2\pi}K_{nn}^{Fx}(\phi_2,\theta_1)u_n(\phi_2)b_2\cos\phi_2\,\mathrm{d}\phi_2,\\
&\cdots\cdots\\
N_{2n} &= \int_0^{\frac{1}{2}\pi}K_{nt}^{Fy}(\phi_2,\theta_1)u_n(\phi_2)b_2\sin\phi_2\cos\phi_2\,\mathrm{d}\phi_2,\\
&\text{for additional hole: } M=1\sim M1\ (0\leqslant\theta_1\leqslant 2\pi).
\end{aligned}
\tag{17a}
$$

$$
\begin{aligned}
A_{1n} &= \int_0^{2\pi}K_{nn}^{Fx}(\phi_1,\theta_2)t_n(\phi_1)b_1\,\mathrm{d}\phi_1,\\
B_{1n} &= \int_0^{2\pi}K_{nn}^{Fx}(\phi_1,\theta_2)t_n(\phi_1)b_1\sin\phi_1\,\mathrm{d}\phi_1,\\
C_{1n} &= \int_0^{2\pi}K_{nn}^{Fx}(\phi_1,\theta_2)t_n(\phi_1)b_1\cos\phi_1\,\mathrm{d}\phi_1,\\
&\cdots\cdots\\
H_{n1} &= \int_0^{2\pi}K_{nn}^{Fy}(\phi_1,\theta_2)u_n(\phi_2)b_1\sin\phi_1\cos\phi_1\,\mathrm{d}\phi_1,\\
C_{2n} &= -\tfrac{1}{2}u_n(\theta_2)\cos^2\theta_{20}+\int_0^{2\pi}K_{nn}^{Fx}(\phi_2,\theta_2)u_n(\phi_2)b_2\cos\phi_2\,\mathrm{d}\phi_2,\\
&\cdots\cdots
\end{aligned}
$$

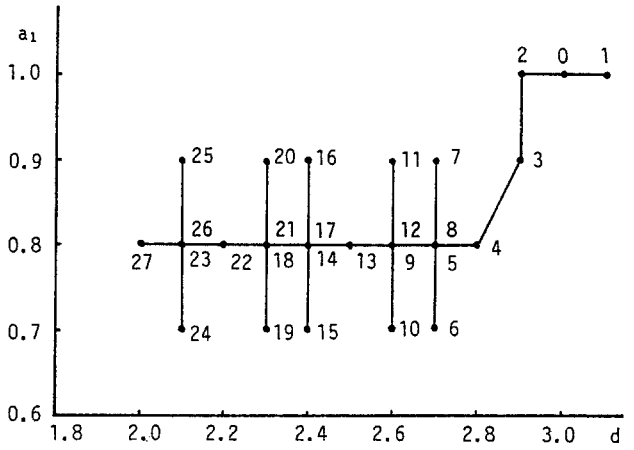

Fig. 5. Example of determination of optimum conditions at the first stage of searching process ($b_1/a_1 = b_2/a_2 = 1$ in Fig. 1).

$$N_{2n} = -\tfrac{1}{2}u_n(\theta_2)\sin^2\theta_{20}\cos\theta_2 + \int_0^{\frac{1}{2}\pi} K_{nt}^{Fy}(\phi_2,\theta_2)u_n(\phi_2)b_2\sin\phi_2\cos\phi_2\,\mathrm{d}\phi_2,$$

$$\text{for principal notch: } M = M1 \sim M1 + M2\ (0 \leqslant \theta_2 \leqslant \tfrac{1}{2}\pi). \tag{17b}$$

The stresses at an arbitrary point are represented by a linear combination of the coefficients a_{1n}, $b_{1n}, \ldots f_{2n}$ and the influence coefficients corresponding to A_{1n}, $B_{1n}, \ldots, N_{2n}$.

The numerical solution is used to determine the stress concentration factors and the stress distribution along the boundaries. In the searching process of the optimum conditions, the direct search method of Hooke and Jeeves is employed [18]. Figure 5 shows an example at the first stage of the searching process in the problem of Fig. 2. After finishing the first stage of the search, the one step length of the parameters in each iteration as shown in Fig. 5 is decreased and the next stage of the search is started.

6. Numerical results and discussion

6.1. Results of the solution of singular integral equations

Table 1 shows the convergence of the unknown functions $\rho_{x1}(\phi_k)$, $\rho_{x2}(\phi_k)$, $\rho_{x3}(\phi_k)$, $\rho_{x4}(\phi_k)$, $\rho_{y1}(\phi_k)$, $\rho_{y2}(\phi_k)$, $\rho_{y3}(\phi_k)$, $\rho_{y4}(\phi_k)$ along the prospective boundary of the additional hole with increasing number of collocation points. Here, the interaction problem between the semicircular notch and two additional circular holes is taken as an example. The present results have converged to 4 digits when $M1 = 12$. Figure 6a shows the variation of the weight functions in comparison with the results of the conventional body force method, where only two unknown functions ρ_x, ρ_y are approximated by using the step-functions when $M1 = 12$, 24. Figure 6b shows the variation of the body force densities in comparison with the results of the conventional body force method when $M1 = 24$. In the present results eight unknown functions of the body force densities, $\rho_{x1}(\phi_k)$, $\rho_{x2}(\phi_k)$, $\rho_{x3}(\phi_k)$, $\rho_{x4}(\phi_k)$, $\rho_{y1}(\phi_k)$, $\rho_{y2}(\phi_k)$, $\rho_{y3}(\phi_k)$, $\rho_{y4}(\phi_k)$ seem to approximate the actual continuous density distributions very well because the present results of $M = 8$ and $M = 12$ coincide with each other to five digit accuracy. On the other hand, two unknown functions ρ_x, ρ_y do not converge with increasing

Table 1. Convergency of unknown functions along the circular boundary in Fig. 1 ($b_1/a_1 = b_2/a_2 = 1$, $a_1/\rho = 0.30$, $d/\rho = 3.03$, $1/\rho = 0.55$)

θ	$M1$	ρ_{x_1}	ρ_{x_2}	ρ_{x_3}	ρ_{x_4}	ρ_{y_1}	ρ_{y_2}	ρ_{y_3}	ρ_{y_4}
	12	0.0476	−0.3919	2.5574	−0.0663	−0.1403	−0.7867	−0.3675	−0.0490
0°	16	0.0465	−0.3886	2.5559	−0.0950	−0.1499	−0.7770	−0.3666	−0.0462
	20	0.0466	−0.3890	2.5561	−0.0911	−0.1488	−0.7780	−0.3666	−0.0465
	24	0.0466	−0.3889	2.5561	−0.0912	−0.1489	−0.7779	−0.3666	−0.0465
	12	0.0310	−0.3846	2.5990	−0.1138	−0.1520	−0.8122	−0.3678	−0.0399
20°	16	0.0315	−0.3835	2.6005	−0.1267	−0.1468	−0.8134	−0.3685	−0.0382
	20	0.0314	−0.3834	2.6005	−0.1262	−0.1479	−0.8129	−0.3683	−0.0383
	24	0.0314	−0.3834	2.6005	−0.1261	−0.1478	−0.8130	−0.3383	−0.0383
	12	−0.0020	−0.3734	2.7426	−0.2413	−0.1081	−0.9278	−0.3798	−0.0125
40°	16	−0.0014	−0.3741	2.7411	−0.2323	−0.1039	−0.9308	−0.3803	−0.0132
	20	−0.0014	−0.3740	2.7415	−0.2331	−0.1030	−0.9313	−0.3803	−0.0131
	24	−0.0014	−0.3739	2.7415	−0.2332	−0.1031	−0.9313	−0.3803	−0.0131
	12	−0.0237	−0.3733	2.9730	−0.3990	0.0700	−1.1481	−0.4131	0.0270
60°	16	−0.0247	−0.3732	2.9722	−0.3998	0.0591	−1.1420	−0.4120	0.0263
	20	−0.0247	−0.3731	2.9718	−0.3987	0.0584	−1.1416	−0.4118	0.0262
	24	−0.0247	−0.3732	2.9717	−0.3986	0.0585	−1.1417	−0.4118	0.0262
	12	−0.0287	−0.3805	3.1618	−0.5092	0.2598	−1.3429	−0.4462	0.0574
80°	16	−0.0283	−0.3805	3.1788	−0.5385	0.2661	−1.3465	−0.4471	0.0601
	20	−0.0283	−0.3804	3.1811	−0.5424	0.2664	−1.3467	−0.4470	0.0603
	24	−0.0283	−0.3804	3.1813	−0.5428	0.2664	−1.3467	−0.4470	0.0603
	12	−0.0289	−0.3819	3.1901	−0.5248	0.2904	−1.3727	−0.4514	0.0618
90°	16	−0.0279	−0.3820	3.2113	−0.5594	0.3021	−1.3796	−0.4529	0.0653
	20	−0.0278	−0.3819	3.2145	−0.5648	0.3035	−1.3804	−0.4529	0.0657
	24	−0.0278	−0.3819	3.2149	−0.5649	0.3036	−1.3805	−0.4529	0.0657

the collocation points as shown in Fig. 6a. The reason is that ρ_x, ρ_y cannot represent density distribution $\rho_x^*(\phi_k)$, $\rho_y^*(\phi_k)$ accurately enough, especially near $\theta_1 = 0$, $\frac{1}{2}\pi$, π, $\frac{3}{2}\pi$ because of the characteristic of the fundamental density functions $n_x(\phi_k)$, $n_y(\phi_k)$ [15–17].

To investigate the satisfaction of the boundary conditions ($\sigma_n = 0$, $\tau_{nt} = 0$), the stresses σ_n, σ_t, τ_{nt} along the additional hole boundary and the semicircular notch have been investigated as shown in Table 2. The values of σ_n, τ_{nt} which should be 0 along the boundary are less than 10^{-5} even when $M1 = 20$ and $M2 = 12$. Therefore, in the present analysis, the boundary requirements can be highly satisfied anywhere along the boundary.

Table 3 shows an example of results when the size and location of additional holes vary at the final process in searching of optimum conditions. Here, the stresses at the points A ($\theta_2 = 90°$) of the semicircular notch and ($\theta_1 = 267.1° \sim 267.3°$) and C ($\theta_1 = 83.7° \sim 83.9°$) of the additional circular hole are shown. In Table 3 is found the effect of varying the defining geometric parameters on the magnitude and the position of maximum stress is shown.

Figure 7 shows an example of stress distribution σ_t along the semi-circular notch and the circular holes shown in Fig. 1 boundary. The solid line shows the stress distribution under the optimum condition ($a_1/\rho = 0.30$, $d/\rho = 3.03$, $1/\rho = 0.55$). The broken line shows the stress distribution for the semi-circular notch without holes (Fig. 7a) and for the circular hole

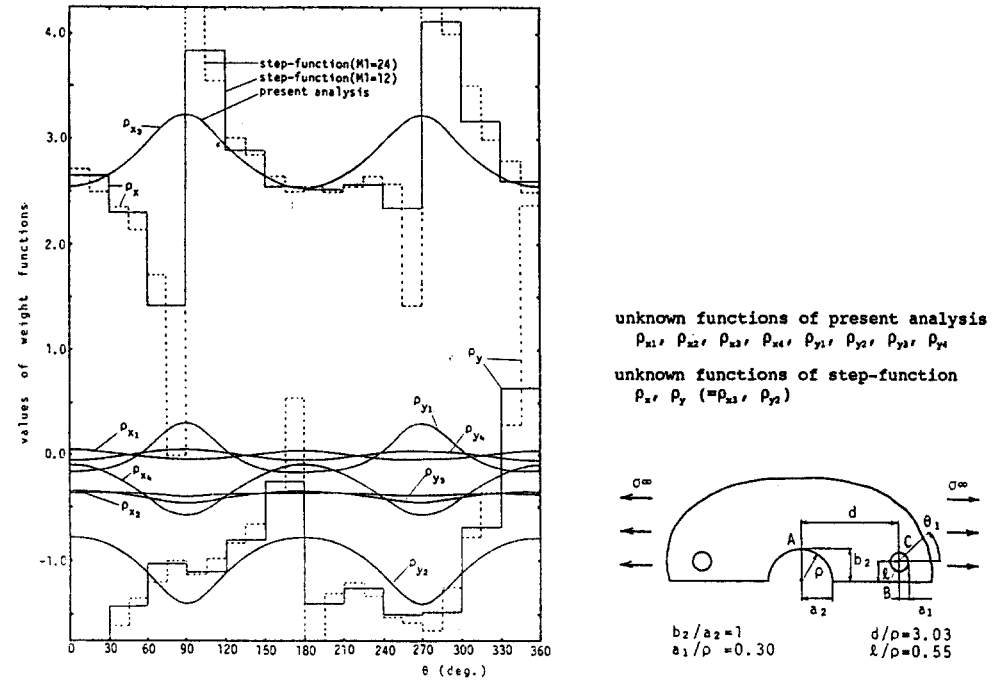

(a)

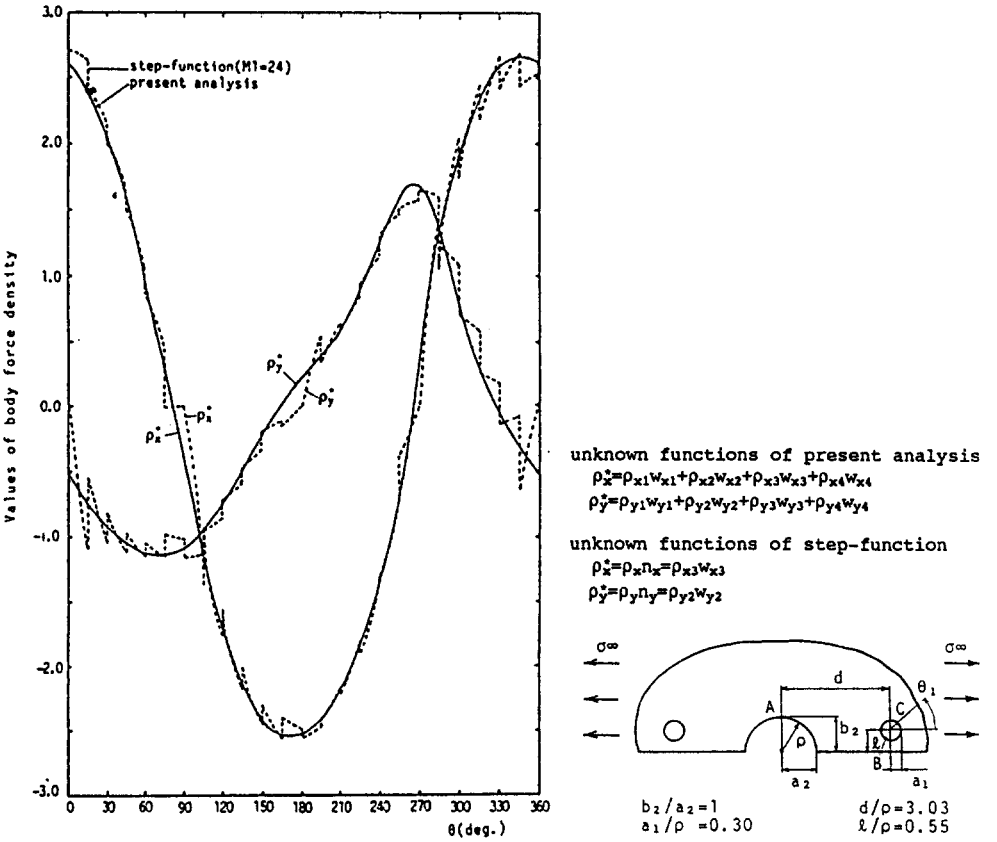

(b)

Fig. 6. Variation of unknown functions in comparison with the conventional body force method: (a) Variation of the weight functions; (b) Variation of the density functions.

Table 2. Convergency of the stresses along the circular boundary and semicircular boundary in Fig. 1 ($b_1/a_1 = b_2/a_2 = 1$, $a_1/\rho = 0.30$, $d/\rho = 3.03$, $l/\rho = 0.55$)

θ	$M1$	σ_t	σ_n	τ_{nt}	$M2$	σ_t	σ_n	τ_{nt}
	12	−0.9800	-9.0×10^{-4}	-2.8×10^{-3}	4	0.0000	7.1×10^{-2}	3.1×10^{-4}
0°	16	−0.9778	7.3×10^{-5}	3.4×10^{-4}	8	0.0000	1.4×10^{-2}	-6.6×10^{-5}
	20	−0.9777	-5.0×10^{-6}	-3.6×10^{-5}	12	0.0000	8.2×10^{-4}	-1.8×10^{-5}
	24	−0.9777	3.0×10^{-7}	3.6×10^{-6}	16	0.0000	-1.7×10^{-4}	-2.0×10^{-5}
	12	−0.2741	7.8×10^{-4}	1.0×10^{-3}	4	0.0692	-3.7×10^{-4}	-5.8×10^{-4}
20°	16	−0.2699	-1.5×10^{-4}	-2.3×10^{-4}	8	0.0716	0.0	0.0
	20	−0.2696	1.4×10^{-5}	2.6×10^{-5}	12	0.0735	-7.0×10^{-8}	-1.4×10^{-7}
	24	−0.2696	-6.6×10^{-7}	-1.4×10^{-6}	16	0.0738	8.8×10^{-9}	1.4×10^{-8}
	12	0.9332	9.5×10^{-4}	6.3×10^{-4}	4	0.8744	2.0×10^{-4}	2.2×10^{-4}
40°	16	0.9310	1.6×10^{-4}	1.3×10^{-4}	8	0.8799	0.0	0.0
	20	0.9312	-1.6×10^{-5}	-1.4×10^{-5}	12	0.8810	2.3×10^{-9}	2.2×10^{-9}
	24	0.9312	-9.8×10^{-7}	-9.6×10^{-6}	16	0.8812	5.5×10^{-11}	4.6×10^{-11}
	12	2.1091	-2.1×10^{-3}	-5.8×10^{-4}	4	2.0071	-2.0×10^{-4}	-1.1×10^{-4}
60°	16	2.1108	-1.2×10^{-4}	-4.2×10^{-5}	8	2.0123	0.0	0.0
	20	2.1108	1.2×10^{-5}	4.9×10^{-6}	12	2.0132	-3.7×10^{-10}	-1.9×10^{-10}
	24	2.1108	2.3×10^{-5}	1.1×10^{-6}	16	2.0133	-1.9×10^{-11}	1.7×10^{-11}
	12	2.7149	-1.1×10^{-3}	-2.2×10^{-5}	4	2.8079	4.6×10^{-3}	7.6×10^{-5}
80°	16	2.7115	4.3×10^{-5}	9.4×10^{-7}	8	2.8126	0.0	0.0
	20	2.7112	-4.5×10^{-6}	-2.5×10^{-7}	12	2.8134	3.7×10^{-10}	5.9×10^{-11}
	24	2.7111	-1.3×10^{-6}	-1.1×10^{-7}	16	2.8135	6.1×10^{-13}	-2.5×10^{-13}
	12	2.6878	2.1×10^{-3}	-3.6×10^{-4}	4	2.9208	7.7×10^{-4}	6.3×10^{-7}
90°	16	2.6826	2.5×10^{-4}	-3.3×10^{-5}	8	2.9249	1.6×10^{-7}	1.8×10^{-10}
	20	2.6820	2.6×10^{-5}	-2.8×10^{-6}	12	2.9257	-1.5×10^{-7}	9.5×10^{-10}
	24	2.6819	2.5×10^{-6}	-2.2×10^{-7}	16	2.9258	-1.8×10^{-11}	1.1×10^{-11}
	12	2.9224	-7.3×10^{-3}	-4.2×10^{-5}				
267.2°	16	2.9234	-8.0×10^{-4}	-1.9×10^{-5}				
	20	2.9235	-7.8×10^{-5}	-3.1×10^{-6}				
	24	2.9236	-7.3×10^{-6}	-3.6×10^{-7}				

Table 3. Example of determination of optimum conditions at the final stage of searching process ($b_1/a_1 = b_2/a_2 = 1$ in Fig. 2)

a_1/ρ	d/ρ	l/ρ	σ_{tA}	σ_{tB}	θ_1	σ_{tC}	θ_1
0.30	3.03	0.55	2.9258	2.9235	267.2°	2.7275	83.9°
0.29	3.03	0.55	2.9361	2.8657	267.2°	2.7122	83.7°
0.31	3.03	0.55	2.9150	2.9853	267.3°	2.7431	83.8°
0.30	3.02	0.55	2.9260	2.9188	267.2°	2.7266	83.8°
0.30	3.04	0.55	2.9261	2.9278	267.2°	2.7286	83.8°
0.30	3.03	0.54	2.9249	2.9521	267.3°	2.7263	83.7°
0.30	3.03	0.56	2.9266	2.8970	267.1°	2.7291	83.7°

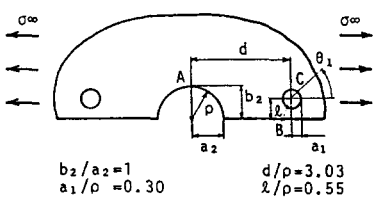

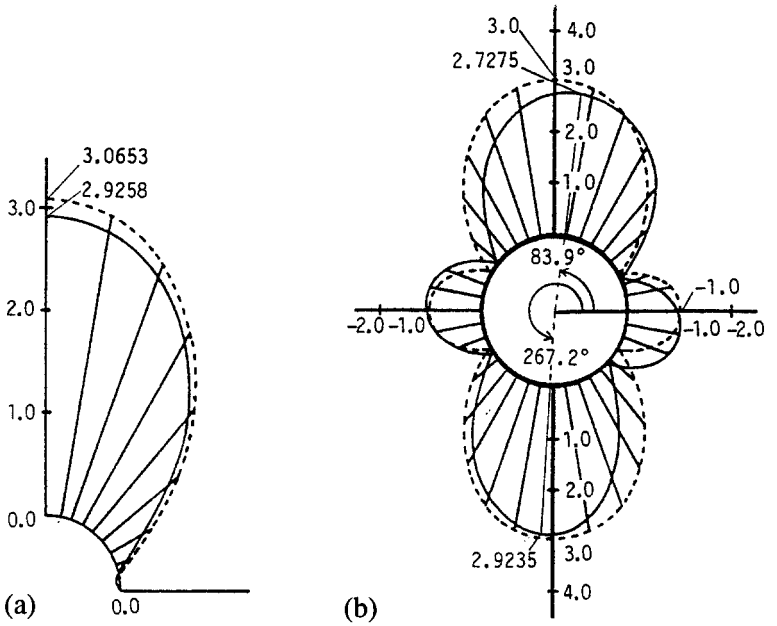

Fig. 7. Example of stress distribution σ_t along the boundary in Fig. 1 ($b_1/a_1 = b_2/a_2 = 1$, $a_1/\rho = 0.30$, $d/\rho = 3.03, 1/\rho = 0.55$): (a) Principal semi-circular notch (- - - -: Stress distribution without holes); (b) Additional circular hole (- - - -: Stress distribution without notch).

Table 4. Optimum conditions of two additional holes in Fig. 1

b_2/ρ	a_1/ρ	d/ρ	l/ρ	σ_{tA}	σ_{tB}	θ_1	σ_{tC}	θ_1	σ_{t0}
1	0.30	3.03	0.55	2.926	2.924	267.2°	2.728	84.0°	3.065
1.5	0.70	3.60	1.30	3.076	2.890	263.4°	3.066	84.0°	3.545
2	1.25	3.77	2.80	3.405	3.312	258.0°	3.405	87.6°	3.951
4	2.30	5.40	4.45	3.494	3.054	253.0°	3.502	86.1°	5.220

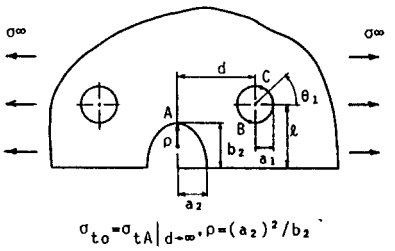

without notch (Fig. 7b). Through the present method, the stress distribution and the optimum conditions can be obtained very accurately.

6.2. Optimum condition for additional stress-relieving holes

Table 4 shows the optimum condition of two additional circular holes for the several aspect ratios a/b of principal semi-elliptical notch. Here, the stresses at the points A ($\theta_2 = 90°$) of the semicircular notch and the points B ($\theta_1 = 253.0° \sim 267.2°$) and C ($\theta_1 = 84.0° \sim 87.6°$) of additional circular holes are shown.

Table 5 shows the optimum condition of two additional elliptical holes for the several aspect ratios of principle and additional ellipse. Here, the stresses at the points A ($\theta_2 = 90°$) of the principle elliptical hole and B ($\theta_1 = 81.7° \sim 86.0°$) of the additional elliptical hole are also shown. According to Shibahara–Taniguchi's results [7], it was decided that $a1 = 0.85a2$, $d = 2.17a2$ and the maximum stress is 2.417 for the circular holes ($b1/a1 = b2/a2 = 1$); however, their results were found to have a few percent errors through the comparison with the present results.

Table 5. Optimum conditions of two additional holes in Fig. 2

b_2/a_2	b_1/a_1	b_1/a_2	d/a_2	σ_{tA}	σ_{tB}	θ_1	σ_{t0}
1	1	0.82	2.02	2.417	2.411	81.7°	3.000
		(0.85)	(2.17)	(2.462)	(2.462)		
2	1	2.25	3.83	2.596	2.596	48.0°	5.000
2	2	1.72	3.05	3.800	3.799	86.0°	5.000

( ): Shibahara–Taniguchi [7]

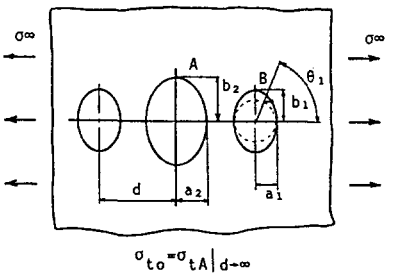

Table 6. Optimum conditions of two additional holes in Fig. 3

b_2/ρ	a_1/ρ	d/ρ	l/ρ	σ_{tA}	σ_{tB}	θ_1	σ_{tC}	θ_1	σ_{t0}
1	0.40	2.95	0.54	2.749	2.001	269.3°	2.747	82.5°	3.000
1.5	0.81	3.95	1.14	2.904	2.526	269.5°	2.906	83.0°	3.449
2	1.28	5.20	1.71	2.988	2.712	269.8°	2.989	84.0°	3.828
4	2.55	5.85	3.48	3.342	3.020	220.0°	3.341	82.1°	5.000

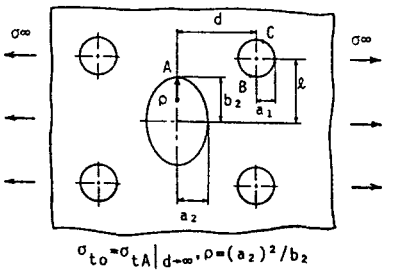

Table 6 shows the optimum condition of four additional circular holes for the several aspect ratios of a principle elliptical hole. Here, the stresses at the points A ($\theta_2 = 90°$) of the principle elliptical hole and B ($\theta_1 = 82.1° \sim 84.0°$) of the additional elliptical hole are also shown.

7. Conclusion

In this paper, a singular integral equation method in optimizing size and location of stress-relieving holes is discussed. The conclusions are summarized as follows:

(1) The intersection problems between principle notch and additional stress-relieving holes were formulated in terms of singular integral equations with Cauchy-type singularities. To formulate the problem, the body force method was applied, where the Green's function for a point force and a force doublet were used as the fundamental solutions.

(2) Numerical solutions of the singular integral equations were considered. In the present analysis, the unknown functions of the body force densities were approximated by a linear combination of products of fundamental density functions and weight functions. To satisfy the boundary condition along the elliptical hole under general loading, eight kinds of fundamental density functions of the body force in the x- and y-directions were applied. The boundary condition was found to be highly satisfied by the present method for several problems.

(3) In the conventional body force method, it was found that the values of two types of body force densities do not converge with increasing collocation points. The reason is that two types of body forces cannot represent real density distribution enough near the apex of an elliptical boundary.

(4) The optimum conditions for stress-relieving holes are obtained accurately through the present method and they are shown in tables for the following problems:

(A) A semi-elliptical notch and two additional circular holes in a semi-infinite plate

(B) An elliptical hole and two additional elliptical holes in an infinite plate

(C) An elliptical hole and four additional circular holes in an infinite plate.

Appendix A

The kernel of (1) is expressed as follows:

$$
\begin{aligned}
K_{nn}^{Fx}(\phi_k,\theta_i) &= \sigma_n^{Fx}(\phi_k,\theta_i)\\
&= \sigma_x^{Fx}(\phi_k,\theta_i)\cos^2\theta_i + \sigma_y^{Fx}(\phi_k,\theta_i)\sin^2\theta_i\\
&\quad +2\tau_{xy}^{Fx}(\phi_k,\theta_i)\sin\theta_i\cos\theta_i\\
K_{nn}^{Fy}(\phi_k,\theta_i) &= \sigma_n^{Fy}(\phi_k,\theta_i)\\
&= \sigma_x^{Fy}(\phi_k,\theta_i)\cos^2\theta_i + \sigma_y^{Fy}(\phi_k,\theta_i)\sin^2\theta_i\\
&\quad +2\tau_{xy}^{Fy}(\phi_k,\theta_i)\sin\theta_i\cos\theta_i,\\
K_{nt}^{Fx}(\phi_k,\theta_i) &= \tau_{nt}^{Fx}(\phi_k,\theta_i)\\
&= (-\sigma_x^{Fx}(\phi_k,\theta_i) + \sigma_y^{Fx}(\phi_k,\theta_i)\sin\theta_i\cos\theta_i\\
&\quad +2\tau_{xy}^{Fx}(\phi_k,\theta_i)(\cos^2\theta_i - \sin^2\theta_i),\\
K_{nt}^{Fy}(\phi_k,\theta_i) &= \tau_{nt}^{Fy}(\phi_k,\theta_i)\\
&= (-\sigma_x^{Fy}(\phi_k,\theta_i) + \sigma_y^{Fy}(\phi_k,\theta_i))\sin\theta_i\cos\theta_i\\
&\quad +2\tau_{xy}^{Fy}(\phi_k,\theta_i)(\cos^2\theta_i - \sin^2\theta_i),
\end{aligned}
\tag{A-1}
$$

where

$$
\begin{aligned}
\sigma^{Fx}(\phi_k,\theta_i) &= \sigma^{Fx1}(\phi_k,\theta_i) + \sigma^{Fx2}(\phi_k,\theta_i),\\
\sigma^{Fy}(\phi_k,\theta_i) &= \sigma^{Fy1}(\phi_k,\theta_i) + \sigma^{Fy2}(\phi_k,\theta_i),
\end{aligned}
\tag{A-2}
$$

$$
\begin{aligned}
\sigma_x^{Fx1} &= \sum_{j=1}^{2}\frac{A}{2\pi(\kappa+1)y(A^2+m^2)^2}[\kappa(A^2+m^2)+(3A^2-m^2)],\\
\sigma_y^{Fx1} &= \sum_{j=1}^{2}\frac{-A}{2\pi(\kappa+1)y(A^2+m^2)^2}[\kappa(A^2+m^2)+(-A^2-5m^2)],\\
\tau_{xy}^{Fx1} &= \sum_{j=1}^{2}\frac{m}{2\pi(\kappa+1)y(A^2+m^2)^2}[\kappa(A^2+m^2)+(3A^2-m^2)],
\end{aligned}
\tag{A-3}
$$

$$
\begin{aligned}
\sigma_x^{Fy1} &= \sum_{j=1}^{2}\frac{-m}{2\pi(\kappa+1)y(A^2+m^2)^2}[\kappa(A^2+m^2)+(-5A^2-m^2)],\\
\sigma_y^{Fy1} &= \sum_{j=1}^{2}\frac{m}{2\pi(\kappa+1)y(A^2+m^2)^2}[\kappa(A^2+m^2)+(-A^2+3m^2)],\\
\tau_{xy}^{Fy1} &= \sum_{j=1}^{2}\frac{A}{2\pi(\kappa+1)y(A^2+m^2)^2}[\kappa(A^2+m^2)+(-A^2+3m^2)],
\end{aligned}
\tag{A-4}
$$

$$
\begin{aligned}
\sigma_x^{Fx2} &= \sum_{j=1}^{2} \frac{A}{2\pi(\kappa+1)y(A^2+n^2)^3}[\kappa\{3A^4+(6n^2-4n)A^2+(3n^4-4n^3)\} \\
&\quad +\{A^4-(10n^2-4n-8)A^2-(11n^4-36n^3+24n^2)\}], \\
\sigma_y^{Fx2} &= \sum_{j=1}^{2} \frac{A}{2\pi(\kappa+1)y(A^2+n^2)^3}[\kappa\{A^4+(2n^2-4n)A^2+(n^4+4n^3)\} \\
&\quad +\{-A^4-(6n^2-12n+8)A^2-(5n^4+20n^3-24n^2)\}], \\
\tau_{xy}^{Fx2} &= \sum_{j=1}^{2} \frac{1}{2\pi(\kappa+1)y(A^2+n^2)^3}[\kappa\{-(n+2)A^4-2n^3A^2-(n^5-2n^4)\} \\
&\quad +\{-(3n-2)A^4-(2n^3-24n^2+24n)A^2+(n^5-10n^4+8n^3)\}],
\end{aligned}
\tag{A-5}
$$

$$
\begin{aligned}
\sigma_x^{Fy2} &= \sum_{j=1}^{2} \frac{-1}{2\pi(\kappa+1)y(A^2+n^2)^3}[\kappa\{(3n+2)A^4+6n^3A^2+(3n^5-2n^4)\} \\
&\quad +\{-(7n-6)A^4-(2n^3-24n^2+24n)A^2+(5n^5-14n^4+8n^3)\}], \\
\sigma_y^{Fy2} &= \sum_{j=1}^{2} \frac{1}{2\pi(\kappa+1)y(A^2+n^2)^3}[\kappa\{-(n-2)A^4-2n^3A^2-(n^5+2n^4)\} \\
&\quad +\{(n-2)A^4-(2n^3-24n^2+24n)A^2-(3n^5+6n^4-8n^3)\}], \\
\tau_{xy}^{Fy2} &= \sum_{j=1}^{2} \frac{-A}{2\pi(\kappa+1)y(A^2+n^2)^3}[\kappa\{A^4+(2n^2-4n)A^2+(n^4-4n^3)\} \\
&\quad +\{-A^4+(2n^2+4n-8)A^2+(3n^4-28n^3+24n^2)\}],
\end{aligned}
\tag{A-6}
$$

where

$$
\begin{aligned}
&A=\frac{\xi_k-x_i}{y_i}(j=1), \quad A=-\frac{\xi_k+x_i}{y_i}(j=2), \\
&m=\frac{\eta_k-y_i}{y_i}, \quad n=\frac{\eta_k+y_i}{y_i}, \\
&r_1=\sqrt{(\xi_k-x_i)^2+(\eta_k-y_i)^2}, \quad r_2=\sqrt{(\xi_k-x_i)^2+(\eta_k+y_i)^2},
\end{aligned}
\tag{A-7}
$$

$$
\kappa=\begin{cases}\dfrac{3-\nu}{1+\nu} & \text{(plane strain)} \\ 3-4\nu & \text{(plane stress)}\end{cases},
\tag{A-8}
$$

$$
\begin{aligned}
&\begin{cases}x_1=d+a_1\cos\theta_1 \\ y_1=l+a_1\sin\theta_1\end{cases} \quad \begin{cases}x_2=a_2\cos\theta_2 \\ y_2=b_2\sin\theta_2\end{cases} \\
&\begin{cases}\xi_1=d+a_1\cos\phi_1 \\ \eta_1=l+b_1\sin\phi_1\end{cases} \quad \begin{cases}\xi_2=a_2\cos\phi_2 \\ \eta_2=b_2\sin\phi_2\end{cases}
\end{aligned}
\tag{A-9}
$$

Appendix B

It can be shown that the kernels $\sigma^{Fx1}(\phi_k, \theta_i)$, $\sigma^{Fy1}(\phi_k, \theta_i)$ have the singularity of the form $1/\{\sin(\theta_i - \phi_i)/2\}$. Then, the following method of evaluation of integrals is applied. Here, $K_{nn}^{Fx}(\phi_1, \theta_1)$, $\rho_{x1}(\phi_1)$ is taken as an example.

$$\begin{aligned} I &= \fint_0^{2\pi} K_{nn}^{Fx}(\phi_1, \theta_1)\rho_{x1}(\phi_1)b_1 \,\mathrm{d}\phi_1 \\ &= \int_0^{\theta-\varepsilon_0} K_{nn}^{Fx}(\phi_1, \theta_1)\rho_{x1}(\phi_{x1})b_1\phi_1 + \fint_{\theta-\varepsilon_0}^{\theta+\varepsilon_0} K_{nn}^{Fx}(\phi_1, \theta_1)\rho_{x1}(\phi_{x1})b_1 \,\mathrm{d}\phi_1 \\ &\quad + \int_{\theta+\varepsilon_0}^{2\pi} K_{nn}^{Fx}(\phi_1, \theta_1)\rho_{x1}(\phi_{x1})b_1 \,\mathrm{d}\phi_1 \\ &= I_1 + I_2 + I_3. \end{aligned} \tag{B-1}$$

The first and third integral can be easily evaluated by the numerical integration procedure. The second integral can be expressed as follows by letting $\phi_1 = \theta_1 + \varepsilon$

$$\begin{aligned} I_2 &= \fint_{-\varepsilon_0}^{\varepsilon_0} K_{nn}^{Fx}(\theta_1 + \varepsilon, \theta_1)\rho_{x1}(\theta_1 + \varepsilon)b_1 \,\mathrm{d}\varepsilon \\ &= \fint_{-\varepsilon_0}^{\varepsilon_0} \left(\frac{c_1}{\varepsilon} + c_2 + c_3\varepsilon + c_4\varepsilon^2 + \cdots\right) b_1 \,\mathrm{d}\varepsilon. \end{aligned} \tag{B-2}$$

The first term integral in the right-hand side in (B-2), interpreted as meaning Cauchy's principle value, should be zero. Neglecting the terms of a higher order than ε^2, we find

$$I_2 = 2c_2\varepsilon_0 b_1. \tag{B-3}$$

Then the singular integrals are calculated by determining of the coefficients c_2 in (B-1).

Acknowledgements

The authors are grateful to reviewers for their helpful discussions and suggestions.

References

1. A.J. Durelli, R.L. Lake and E. Phillips, *Proceedings SESA* 10, 1 (1952) 53–64.
2. P.E. Erickson and W.F. Riley, *Experimental Mechanics* 18, 3 (1975) 97–100.
3. V. Tvergaard, *Proceedings IUTAM Symposium on Optimization in Structural Design*, Warsaw (1973).
4. A. Francavilla, C.V. Ramakrishnan and O.Z. Zwinkiewicz, *Journal of Stress Analysis* 10(2) (1975).
5. S.S. Bhavikatti and C.V. Ramakrishnan, *International Journal of Mechanical Science* 21, 1 (1979) 29–39.
6. E. Schnack, *International Journal for Numerical Method in Engineering* 14 (1979) 115–124.
7. M. Shibahara and Y. Taniguchi, *Transactions of the Japan Society of Mechanical Engineers* 49 (1983) 1261–1265.
8. N.A. Noda and H. Umeki and F. Erdogan, *Transactions of the Japan Society of Mechanical Engineers* 55 A (1989) 2521–2526.
9. N.A. Noda and K. Oda, *International Journal of Fracture* 58 (1992) 285–304.
10. N.A. Noda, K. Oda and T. Matsuo, *Localized Damage II, Vol. 2: Computational Method in Fracture Mechanics*, M.H. Adiabadi, H. Nisitani and D.J. Cartwright (eds.), Computational Mechanics Publications, Southampton (1992) 35–56.
11. N.A. Noda and T. Matsuo, *International Journal of Fracture* 63 (1993) 229–245.

12. H. Nisitani, *Journal of the Japan Society of Mechanical Engineers* 70 (1967) 627–632. [*Bulletin of Japan Society of Mechanical Engineers* 11 (1968) 14–23.]
13. H. Nisitani, *Mechanics of Fracture, Vol. 5 Stress Analysis of Notched Problem*, G.C. Sih (ed.), Leyden (1974) 1–68.
14. H. Nisitani and D.H. Chen, *The Body Force Method (Taisekiryokuho in Japanese)*, Baifukan, Tokyo (1987) 89–90.
15. N.A. Noda and T. Matsuo, *Transactions of the Japan Society of Mechanical Engineers* 58–555 A (1992) 2179–2184.
16. N.A. Noda and T. Matsuo, *Transactions of the Japan Society of Mechanical Engineers* 55–559 A (1993) 785–791.
17. N.A. Noda and T. Matsuo, *Fracture Mechanics; 25th Volume, ASTM STP 1220*, F. Erdogan and R.J. Hartranft (eds.) (submitted).
18. S.L.S. Jacoby, J.S. Kowalik and J.T. Pizzo, *Iterative Method for Nonlinear Optimization Problems*, Prentice-Hall, Englewood Cliff (1972).